Heliyon 5 (2019) e02908

Contents lists available at ScienceDirect

Heliyon

journal homepage: www.heliyon.com

Research article

Crystal structures and the electronic properties of silicon-rich silicon carbide materials by first principle calculations

Noura D. Alkhaldi, Sajib K. Barman, Muhammad N. Huda *

Department of Physics, University of Texas Arlington, Box 19059, Arlington, Texas, 76019, USA

ARTICLE INFO

Keywords:
Condensed matter physics
Materials chemistry
Materials science
Si-rich-silicon carbide
Photovoltaic
Density functional theory

ABSTRACT

Silicon carbide has been used in a variety of applications including solar cells due to its high stability. The high bandgap of pristine SiC, necessitates nonstoichiometric silicon carbide materials to be considered to tune the band gap for efficient solar light absorptions. In this regards, thermodynamically stable Si-rich Si_xC_{1-x} materials can be used in solar cell applications without requiring the expensive pure grade silicon or pure grade silicon carbide. In this work, we have used density functional theory (DFT) to examine the stability of various polymorphs of silicon carbide such as 2H–SiC, 4H–SiC, 6H–SiC, 8H–SiC, 10H–SiC, wurtzite, naquite, and diamond structures to produce stable structures of Si-rich Si_xC_{1-x}. We have systematically replaced the carbon atoms by silicon to lower the band gap and found that the configurations of these excess silicon atoms play a significant role in the stability of Si-rich Si_xC_{1-x}. Hence, we have investigated different configurations of silicon and carbon atoms in these silicon carbide structures to obtain suitable Si_xC_{1-x} materials with tailored band gaps. The results indicate that 6H-Si_xC_{1-x} is thermodynamically the most favorable structure within the scope of this study. In addition, Si substitution for C sites in 6H–SiC enhances the solar absorption, as well as shifts the absorption spectra toward the lower photon energy region. In addition, in the visible range the absorption coefficients are much higher than the pristine SiC.

1. Introduction

Silicon carbide is a very important semiconductor material [1, 2] which has more than 200 poly-types [3] and has great properties which make it an attractive material to be used for applications in extreme environment [4, 5, 6]. These interesting properties include high strength, high hardness, and low thermal expansion [7, 8, 9], and it has been used in high-temperature applications because of its high thermal conductivity [10, 11, 12] which is 3.6 W/cm-K for 3C–SiC, and 4.9 W/cm-K for 4H–SiC and 6H–SiC [13]. 3C–SiC, 2H–SiC, 4H–SiC, and 6H–SiC are the most common phases. SiC can be synthesized by chemical vapor deposition (CVD) [14, 15, 16, 17, 18], vapor liquid solid (VLS) [19, 20, 21, 22, 23] and physical vapor transport (PVT) [24, 25, 26, 27, 28] methods. Silicon carbide has been used in photovoltaic solar cells (PVSC) [29, 30, 31, 32, 33, 34, 35] for decades. However, photovoltaic devices need efficient materials which have high stability and suitable band gap to work efficiently. The band gap of SiC ranges from 2.3 eV to 3.3 eV [36, 37, 38, 39, 40]. This is higher than what is suitable for efficient solar energy absorptions. Efficient solar conversion requires a bandgap of less than 1.5 eV. Hence, it is necessary to have tunable band gaps in SiC materials. Previously, it has also been shown from the first principle based atomistic simulations that Si-rich SiC nano-clusters can be very stable and can have tunable energy gaps [41, 42, 43]. In the bulk limit, the non-stoichiometric SiC may provide such options [44] as well, so we have studied Si-rich SiC with periodic boundary conditions in this work.

It has been shown that increasing carbon atoms in amorphous silicon carbide will increase the optical band gap, and the fraction of carbon affects the optical properties negatively in amorphous silicon carbide [45, 46]. Also, the result shows that the optical band gap changes as the silicon concentration increases. A non-stoichiometric Si-rich Si_xC_{1-x} film can increase the percentage of the conversion efficiency of a p-n junction photovoltaic solar cell by up to 3% than that of crystalline silicon within the visible wavelengths (400–600 nm) which is due to enhanced optical absorption. Si-rich Si_xC_{1-x} film can also be used to engineer the visible and near-infrared absorbance and can be enhanced [44, 45, 47]. These results indicate that the absorption coefficient correlates with the ratio of silicon-rich silicon carbide [44, 45]. The experimental result also shows that due to the increasing number of silicon atoms in Si-rich Si_xC_{1-x}, the optical bandgap of the Si-rich Si_xC_{1-x} has been reduced from 2.05 eV to 1.49 eV [44]. The silicon and carbon ratio of the Si-rich Si_xC_{1-x} films can

* Corresponding author.
E-mail address: huda@uta.edu (M.N. Huda).

https://doi.org/10.1016/j.heliyon.2019.e02908
Received 3 March 2019; Received in revised form 10 November 2019; Accepted 20 November 2019

be characterized by utilizing X-ray photoelectron spectroscopy and Mg Kα radiation at 1253.6 eV, and the transmittance and reflectance spectra can be used to analyze the absorption coefficient of Si-rich Si_xC_{1-x} [44]. It has been shown before that the optical absorption capability of non-stoichiometric silicon-rich silicon carbide film is better with reduced optical bandgap than crystalline silicon (c-Si) [44, 47], hence non-stoichiometric Si-rich Si_xC_{1-x} can be used as an alternative to silicon in photovoltaic applications.

The silicon-rich silicon carbide films have been synthesized by using low temperature and low power plasma enhanced CVD (PECVD) method in a system which is rich by the inorganic compound silane [44, 45]. Moreover, silicon-rich silicon carbide has existed as a nonstoichiometric matrix which corresponds to Si fabrication technology to keep the self-assembled Si-quantum dots (QDs) [48].

Si-rich SiC:$Si_{0.74}C_{0.26}$ film has an optical bandgap around 1.45 eV which provides a large absorption coefficient of 3.8×10^5 cm^{-1} in the visible wavelength region. In the limit of all C atoms replaced by Si atoms, the band gap should approach to pure Si gap which is 1.1 eV [47]. However, we would like to avoid the indirect band gap problem which a shortcoming of pristine Si solar cell devices. Due to the tunability of the band gap, this material nowadays is being used in optoelectronic devices such as light-emitting diodes as well [48].

2. Computational methods

The calculations of this work were done within the framework of density functional theory (DFT) as in Vienna ab initio simulation package (VASP) [49, 50]. We have utilized the Projector augmented-wave method (PAW) [51, 52] and generalized gradient approximation [53], namely the Perdew–Burke–Ernzerhof (PBE) as an exchange-correlation functional [54]. We relaxed all the structures before the total energies' calculation. Then, we calculated the formation enthalpies to examine the stability of these structures. The formation enthalpy was calculated using the following formula

$$\Delta H_f = E(Si_xC_y) - xE(Si) - yE(C) \quad (1)$$

where ΔH_f is the formation enthalpy, and $E(Si_xC_y)$ is the total energy of the unit cell of a SiC system, $E(Si)$ is the total energy of the stable bulk diamond phase of Si per atom, and $E(C)$ is the total energy of stable bulk Graphite phase per C atom. x and y represent the total number of Si and C atoms in the unit cell doped or removed, respectively. We included Van der Waals forces in our calculation to determine the total energy of bulk Graphite [55, 56].

We have utilized Materials project [57], and American mineralogist crystal structure database [58] to collect initial structure parameters of 2H, 4H, 6H, diamond, FeSi and wurtzite structures of silicon carbides. VESTA (visualization for electronic and structural analysis) was used throughout the work to visualize all the crystal structures [59]. Tetrahedron method was used to calculate the density of states (DOS) with different denser K-point meshes taking the size of the supercell into account. The kinetic energy cut-off for the plane-wave basis set was set to 400 eV, and all the ions were relaxed until Hellman-Feynman force was equal to or less than 0.01 eV/Å. Note, Gaussian smearing was used when the tetrahedron method was not applicable with some large hexagonal structures.

Due to the prospective applications of Si rich Si_xC_{1-x} materials in photovoltaics, it is important to study its optical absorption under visible light spectrum. Hence the frequency dependent complex dielectric function $\epsilon(\omega) = \epsilon_1(\omega) + i\epsilon_2(\omega)$ is calculated in the independent particle picture using VASP. Here ϵ_1 and ϵ_2 are the real and imaginary parts respectively. ω is the frequency of the incident photon. The expression for $\epsilon_2(\omega)$ is as follow [60]:

$$\varepsilon_2(\omega) = \frac{4\pi^2 e^2}{m\omega^2} \sum_{i,j} \int < i|M|j>^2 f_i\,(1-f_i\,) \times \delta\left(E_{j,k} - E_{i,k} - \omega\right) d^3k \quad (2)$$

In this expression, e and m are the charge and mass of an electron respectively. M is the dipole matrix. i and j are initial and final states respectively. $f_i$is the fermi distribution for the i-th state with wave function vector k. The real part of the dielectric function can be found by the Kramers–Kronig transformation as

$$\varepsilon_1(\omega) = 1 + \frac{2}{\pi} P \int_0^{\infty} \frac{\omega' \varepsilon^2(\omega') d\omega'}{(\omega'^2 - \omega')} \quad (3)$$

Hence, the optical absorption coefficient can be found from the following formula:

$$\alpha(\omega) = \frac{\sqrt{2}\omega}{c} \sqrt{\sqrt{\varepsilon^{1^2} + \varepsilon^{2^2}} - \varepsilon'} \quad (4)$$

3. Results and discussions

3.1. Pristine silicon carbide

At first, we have examined different structures of pristine silicon carbide such as 2H, 4H, 6H, diamond, wurtzite, and FeSi structures of silicon carbides. We utilized the wurtzite structure of zinc sulfide [58] by replacing all zinc atoms with silicon and sulfide atoms with carbon. Naquite structure of FeSi [61] is used where iron atoms are replaced by silicon, and the silicon atoms which are originally in FeSi structure are replaced by carbon atoms. In such unrelaxed naquite-structure of SiC, a Si atom is bonded with seven equivalent C atoms whereas a fully relaxed pure structure transforms into a diamond structure. For the defect studies in naquite structure, we doped Si atoms at C sites in the original unrelaxed form and then relaxed systems without any constraint to check if similar naquite-diamond phase transformation takes place. Hence both naquite and diamond structures are considered for defect studies. Note that a Si atom possesses a tetrahedral coordination with C atoms in a diamond structure. Table 1 shows the lattice parameters of their unit cells after full relaxation. Our optimized lattice parameters are in excellent agreement with the available experimental results [62]. Since GGA overestimates lattice parameters, our calculated results are slightly larger than the experimental results, but in all the cases these are less than 1%.

The calculated formation enthalpies of SiC structures are presented in Table 2. It shows that the diamond and FeSi structures have the same formation enthalpies per atom and are the lowest which indicates that they are the most stable structures, with 6H being slightly less stable by 0.001eV per atom. Given the small energy difference between 6H and cubic SiC structures, at least computationally at the GGA, it is apparent that wurtzite structure has the third lowest formation enthalpy and the 4H being the lowest stable phase for pristine SiC.

3.2. Silicon-rich silicon carbide structures

The main aim of this paper is to study different structures of silicon-rich silicon carbide materials and their stability along with electronic properties. The chemical formula of silicon-rich silicon carbide can be defined as nSi_C:SiC which states n number of carbon atoms are replaced by n silicon atoms in an otherwise pristine silicon carbide phase. Our

Table 1
GGA optimized lattice parameters of pure SiC in 2H, 4H, 6H, diamond, FeSi, and wurtzite structures in their unit cells.

Structure	Lattice parameters					
	a (Å)	b (Å)	c (Å)	α(°)	β (°)	γ (°)
2H	3.086	3.086	5.065	90	90	120
4H	3.094	3.094	10.129	90	90	120
6H	3.094	3.094	15.185	90	90	120
Diamond	4.372	4.372	4.372	90	90	90
FeSi	4.372	4.372	4.372	90	90	90
Wurtzite	3.090	3.090	10.109	90	90	120

Table 2
The formation enthalpies per atom of fully GGA-relaxed SiC phases.

Structure	Formation enthalpy per atom (eV)
2H–SiC	-0.162
4H–SiC	-0.161
6H–SiC	-0.164
Diamond	-0.165
FeSi	-0.165
Wurtzite	-0.163

work mainly focuses on taking off the carbon atoms and substitute them with silicon to get structures having more silicon than the carbon atoms. We have examined all the pristine SiC phases which we have mentioned earlier, namely 2H, 4H, 6H, FeSi, wurtzite and diamond structures, and found that the diamond and 6H structures are among the favorable structures of SiC in this respect. Later we will discuss 8H- and 10H–SiC structures as well. In this section, we doped silicon for carbon sites for the diamond and 6H structures only to check the structural properties after full relaxation. We considered ($2 \times 2 \times 2$) supercells where the pristine diamond structure has 32 silicon and 32 carbon atoms, and the pristine 6H structure has 48 silicon and 48 carbon atoms. First, we made silicon-rich silicon carbides by replacing one carbon with one silicon atom, Si_C:SiC, where $n = 1$. Fig. 1 shows the relaxed structures of diamond and 6H structures of silicon-rich silicon carbides. Then, in the second step we replaced two carbon atoms by two silicon atoms in the structures, $2Si_C$:SiC. We considered different configurations for replacing carbon atoms. For this, we considered situations such as the substituted Si atoms are near to and far from each other (Fig. 2) to examine which structure would be the favorable one.

We have found that the relaxed volume is smaller when the extra silicon atoms are near to each other, and larger when they are far from each other in most of the cases. We continued the same procedure up to eight carbon atoms and replaced them by silicon atoms in the SiC structures in different configurations. It is found that the volume increases progressively as the number of Si atoms are increased in the SiC structures. Note that the volume of the relaxed cells increases faster in the cubic (diamond) structures, which is 16.91% than that in the hexagonal (6H) structures, 9.32% while one to eight Si substitution takes place for C sites. It has also been found that the contribution from covalent bonding in hexagonal structures is higher than that in cubic structures, which will be presented in detail later, and the smaller compact structure of hexagonal structure is a result of that.

To see whether the substitution of extra Si atoms preserves the structural integrity, Table 3 shows the lattice parameters of $2 \times 2 \times 2$ supercells of diamond and 6H structures, respectively. It can be seen that in Si_C:SiC of diamond structure, the lattice parameters a, b, and c are equal, and the angels are also equal which mean that the symmetry did not break through the modeling processes. We have found the symmetry is preserved for 6H structures as well. However, it can also be argued that in diamond structures of nSi_C:SiC ($n = 2$ to 8), the lattice parameters a, b, and c are almost equal and angles' deviation from 90° is very small. Similarly, for 6H nSi_C:SiC ($n = 2$ to 8), the lattice parameter a and b are almost equal and angles' deviation from 90° and 120° is not much. These imply that the overall structural integrity considered for Si-rich SiC are preserved here.

3.3. Formation enthalpies of silicon-rich silicon carbides

After all the structures are fully relaxed, we have calculated the formation enthalpies per atom for nSi_C:SiC ($n = 1$ to 8) in diamond, FeSi, wurtzite and 6H structures, which are presented in Table 4. It is found that the 6H structure of $1Si_C$:SiC has the lowest formation enthalpy which is 0.012 eV per atom lower than that of the diamond structure. When two carbon atoms were replaced by silicon atoms ($2Si_C$:SiC), we examined two different situations for diamond and 6H structures only. In the first case doped Si atoms were placed near to each other and in the second

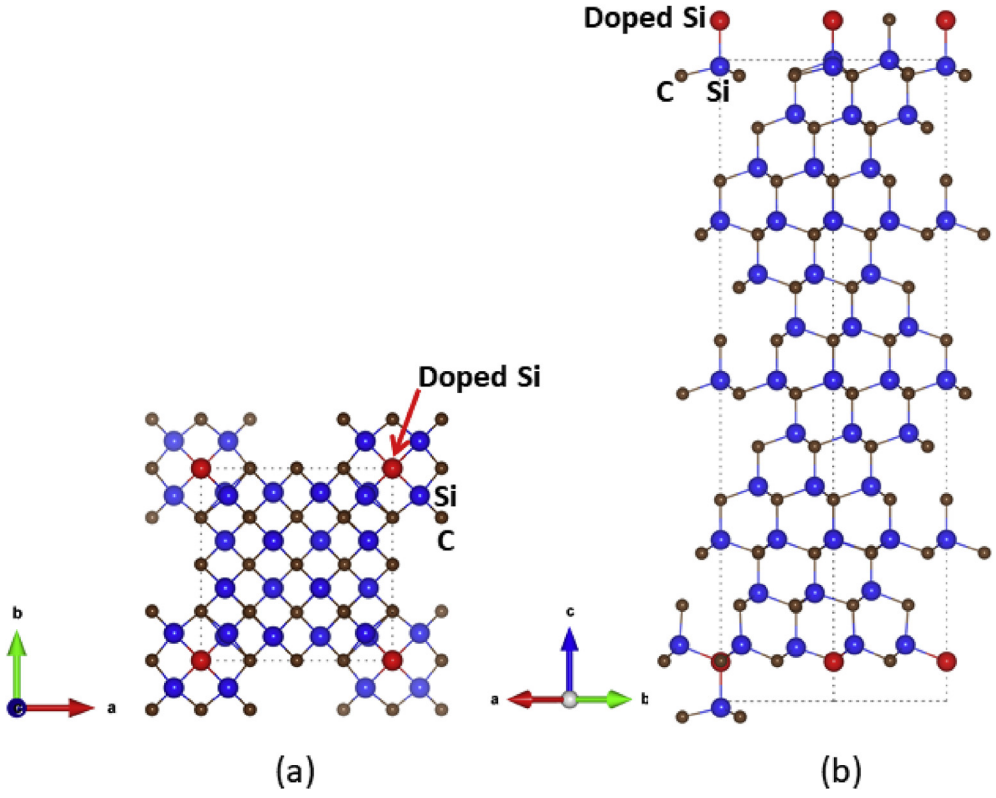

Fig. 1. Silicon-rich silicon carbide of (a) diamond, and (b) 6H structures in their $2 \times 2 \times 2$ supercell representation. Blue for silicon, small brown for carbon and red for extra silicon doped for carbon sites.

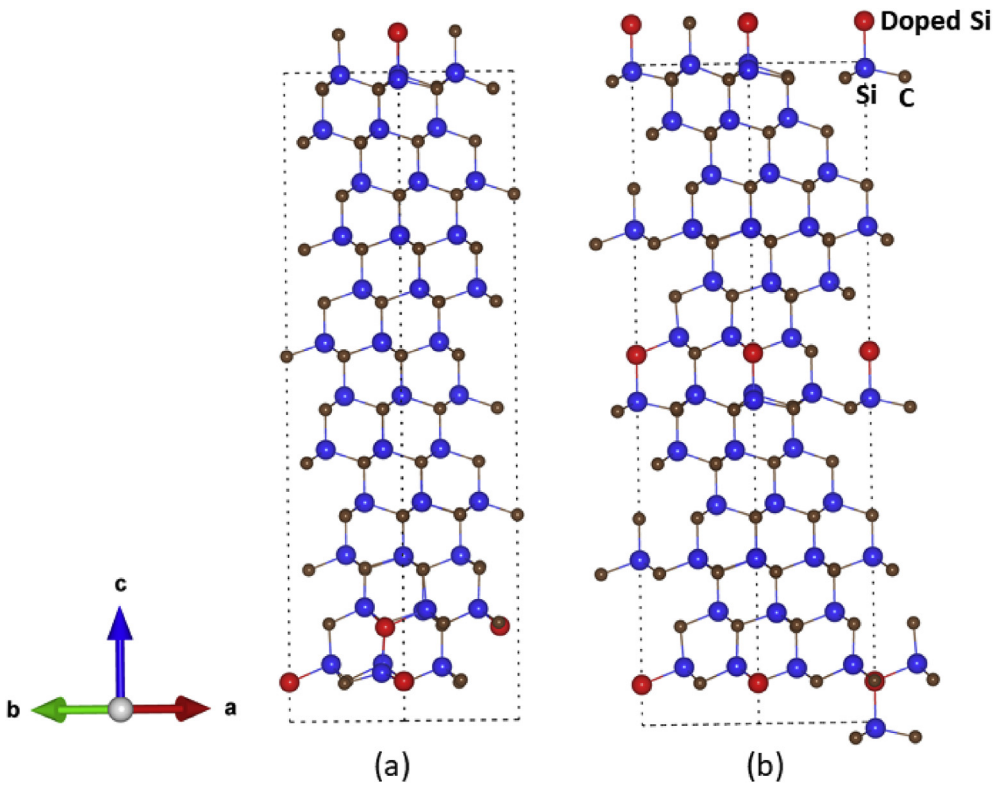

Fig. 2. 6H structure of $2Si_C$:SiC with two extra silicon atoms (a) near and (b) far from each other in 2×2×x2 supercells. Blue for silicon, small brown for carbon and red for extra silicon doped for carbon sites.

Table 3
The lattice parameters of GGA-relaxed diamond and 6H structures for 2 × 2 × 2 supercells for nSi_C:SiC (n = 1 to 8).

Structure	Diamond						6H					
	Lattice parameters						Lattice parameters					
	a (Å)	b (Å)	c (Å)	α (°)	β (°)	γ (°)	a (Å)	b (Å)	c (Å)	α (°)	β (°)	γ (°)
$1Si_C$:SiC	8.812	8.812	8.812	90	90	90	6.210	6.210	30.485	90	90	120
$2Si_C$:SiC	8.887	8.874	8.874	90.193	90	90	6.246	6.240	30.647	90.137	90	120.030
$3Si_C$:SiC	8.947	8.947	8.947	90.207	90.207	89.792	6.272	6.229	30.893	90	90.172	119.773
$4Si_C$:SiC	8.999	9.045	8.987	90	90	90	6.304	6.237	31.070	90	90.431	119.649
$5Si_C$:SiC	9.065	9.099	9.065	90.266	90.032	89.955	6.195	6.194	32.420	90	90.738	119.993
$6Si_C$:SiC	9.145	9.149	9.149	89.734	90	90	6.219	6.195	32.417	91.799	90	120.128
$7Si_C$:SiC	9.203	9.220	9.220	90.263	90.037	89.962	6.185	6.175	33.277	89.409	89.938	119.939
$8Si_C$:SiC	9.280	9.291	9.291	90	90	90	6.165	6.165	33.812	90	90	120

case they were far from each other. The calculated formation enthalpies are less when the extra two silicon are near to each other than when they are far. It is about 0.003 eV less for the 6H structure, and 0.001 eV less for the diamond structure as in Table 5. The reason that formation enthalpies per atom decrease less for the diamond structure is that the Si–Si interaction is less in the diamond structure than that in the 6H structure.

Table 4
The formation enthalpies per atom for diamond, FeSi, wurtzite and 6H structures with silicon substitution for carbon sites.

Structure	Formation enthalpies per atom (eV)			
	Diamond	FeSi	Wurtzite	6H
$1Si_C$:SiC	-0.108	-0.108	-0.098	-0.120
$2Si_C$:SiC	-0.060	-0.059	-0.052	-0.081
$3Si_C$:SiC	-0.014	-0.005	-0.016	-0.068
$4Si_C$:SiC	+0.017	+0.215	-0.006	-0.057
$5Si_C$:SiC	+0.053	+0.118	+0.022	-0.05
$6Si_C$:SiC	+0.098	+0.130	+0.019	-0.040
$7Si_C$:SiC	+0.120	+0.136	+0.075	-0.038
$8Si_C$:SiC	+0.152	+0.137	+0.068	-0.005

Also, for $3Si_C$:SiC, we made different arrangements of the extra three silicon atoms in SiC diamond and 6H structures: when they are close to each other, far from each other and two of them are close to each other and the third one is far from the other two. The calculated the formation enthalpies for all three scenarios can be found in Table 6. The results show that when the extra silicon atoms are close to each other, it gives lower energies than when they are relatively far from each other. The formation enthalpy of the 6H structure is -0.068 eV per atom, which is lower than that of the diamond structure. Similarly, we considered different configurations of distributing the extra silicon atoms in $4Si_C$:SiC

Table 5
Formation enthalpies of 6H and diamond structures of $2Si_C$:SiC. For both cases two Si atoms are doped at C sites in 2 × 2 × 2 supercells of SiC.

Structure	Formation enthalpy per atom (eV)	
	6H	Diamond
2 extra silicon atoms near each other	-0.081	-0.060
2 extra silicon atoms far from each other	-0.078	-0.059

Table 6
Formation enthalpies of 6H and diamond structures of $3Si_C$:SiC. For both cases three Si atoms are doped at C sites in 2 × 2 × 2 supercells of SiC.

Structure	Formation enthalpy per atom (eV)	
	6H	Diamond
3 extra silicon atoms near each other	-0.068	-0.014
3 extra silicon atoms far from each other	-0.040	-0.005
2 extra silicon atoms near each other and one extra far from them	-0.042	-0.004

to see the validity of our expectation about choosing the extra silicon atoms to be close to each other. We examined two different configurations of 6H structure and found the most favorable one formed when all the four doped Si atoms were close to each other (Table 7). The formation enthalpy per atom for the lowest energy structure is -0.057 eV in this case. However, for diamond structure, despite the fact that we have considered numerous configurations (Here, only two cases are presented in Table 7), the formation enthalpies remained positive, which means that $4Si_C$:SiC diamond structures are no longer thermodynamically favorable.

Repeating the above procedure of replacing carbon by silicon atoms we continued up to eight Si atoms. In all these cases, we have found that 6H structure is the most favorable one. The diamond structure as mentioned in the preceding paragraph from 4 substitutional Si atoms formation enthalpies become all positive. Similar trend was shown for FeSi-type structure. However, for Wurtzite structure, after 5^{th} substitutional Si atom, formation enthalpies became all positive. Only the 6H SiC structure has shown the thermodynamic stability up to 8 substitutional Si atoms in SiC (Table 4).

It can be seen from Fig. 3 that up to $8Si_C$:SiC, the 6H structure has the lowest formation enthalpies per atom compared to all other structures, and the only structure with all negative formation enthalpies. The trend shows that out of all Si-rich structures 6H structures are thermodynamically stable. However, it should be noted here that in the case where all carbon atoms are replaced by silicon atoms which is the Si bulk limit, the diamond structure is the ground state structure. The figure also shows that the formation enthalpy has similar trend for diamond, wurtzite, and FeSi structures for up to 3 extra Si atoms, while 6H structure takes a different path.

Table 4 summarizes the formation enthalpies of this Si-rich nSi_C:SiC structures for 6H, wurtzite, FeSi and diamond structures. We did not consider 2H and 4H in our calculations because it gives positive formation enthalpies even for a single C replaced by a Si atom. Also, we have noticed that cubic structures, namely diamond, and FeSi structures started to give positive formation enthalpy when four carbon atoms are replaced by silicon atoms. It means those structures were no longer thermodynamically stable. We also tried several arrangements of extra silicon atoms to examine it further. However, it was not the case with 6H structures which gave negative formation energies up to eight carbon atoms replaced by silicon atoms. We noticed that the carbon atoms which were replaced by silicon atoms should be near to each other either at the same layer or same plane to get the lowest energy structure for a given number of extra Si atoms.

At this point, we carried out calculations for higher order hexagonal

Table 7
Formation enthalpies of 6H and diamond structures of $4Si_C$:SiC. Four Si atoms (two pairs) are doped at C sites in 2 × 2 × 2 supercells of SiC.

Structure	Formation enthalpy per atom (eV)	
	6H	Diamond
2 pairs of Si atoms where one pair is far from the other	-0.013	0.046
Both pairs are close to each other	-0.057	0.036

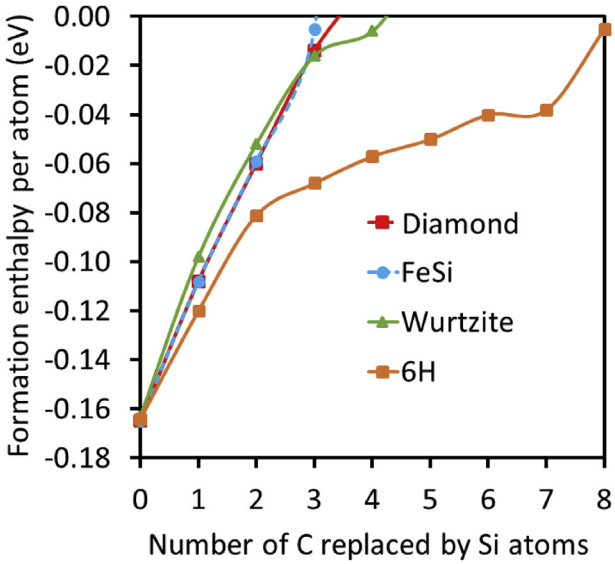

Fig. 3. Comparing the formation enthalpies of 6H, diamond, wurtzite, and FeSi structures of silicon-rich silicon carbide materials.

structures such as 8H and 10H structures for both pristine and silicon-rich silicon carbides. In 8H and 10H structures, $\alpha = \beta = 90^{\circ}$ and $\gamma = 120^{\circ}$. After full relaxation, we found that for 8H, the lattice parameters for the pristine structure are a = b = 3.095 A° and c = 20.242 A°; where a and b in 10H are the same as in 8H but c = 25.301 A°. Our calculations also reveal that the volume of silicon-rich silicon carbides of both 8H and 10H structures increase after full relaxation as Si is doped for C sites. In 8H, the lattice parameter c increases from 20.242 A° to 21.478 A° while in 10H it increases from 25. 301 A° to 26.581 A°. We calculated the formation enthalpies for both 8H (Si_8C_8) and 10H ($Si_{10}C_{10}$) structures [63] and found that their stability are the same for pure phases and it is -0.1645 eV per atom, which is also comparable to 6H. However, for silicon-rich silicon carbide ($1Si_C$:SiC), we find that 10H structure tends to give the lowest formation enthalpy which equals to -0.042 eV per atom. The energetics are reported in Table 8.

Out of all the possible arrangements that we have considered in this work, our investigation suggests that substituted silicon atoms like to stay in the same layer and distribute symmetrically along *a* and *b*. However, these want to stay as far as possible along *c*.

Stability of these structures can also be assessed from another point of view. Electrostatic energy is the potential energy which comes from Coulomb forces due to the ionic nature of the crystal structures and can be found by carrying out Ewald summation over the positive and negative ions as in [64]. We calculated the electrostatic energies for both pure and silicon-rich silicon carbide structures of this work. It is well-known that SiC has both covalent and ionic bonding in the structure due to the electronegativity difference between Si and C atoms. In pure relaxed form, since diamond and FeSi–SiC structures have exactly same geometry, their electrostatic energies are same. Hence, electrostatic energy for pure diamond structure is reported only in Fig. 4 (a). The figure shows that pure diamond SiC has the lowest electrostatic energy. Now, due to extra Si substitution, there should be an overall reduction of electrostatic energy. Fig. 4 (b) shows the calculated electrostatic energies for

Table 8
Formation enthalpies for 8H and 10H pure and nSi_C:SiC structures.

Structure	Formation enthalpy of SiC per atom (eV)	Formation enthalpy of Si-rich SiC per atom (eV) (one C replaced by Si per unit cell)
8H	-0.1645	-0.012
10H	-0.1645	-0.042

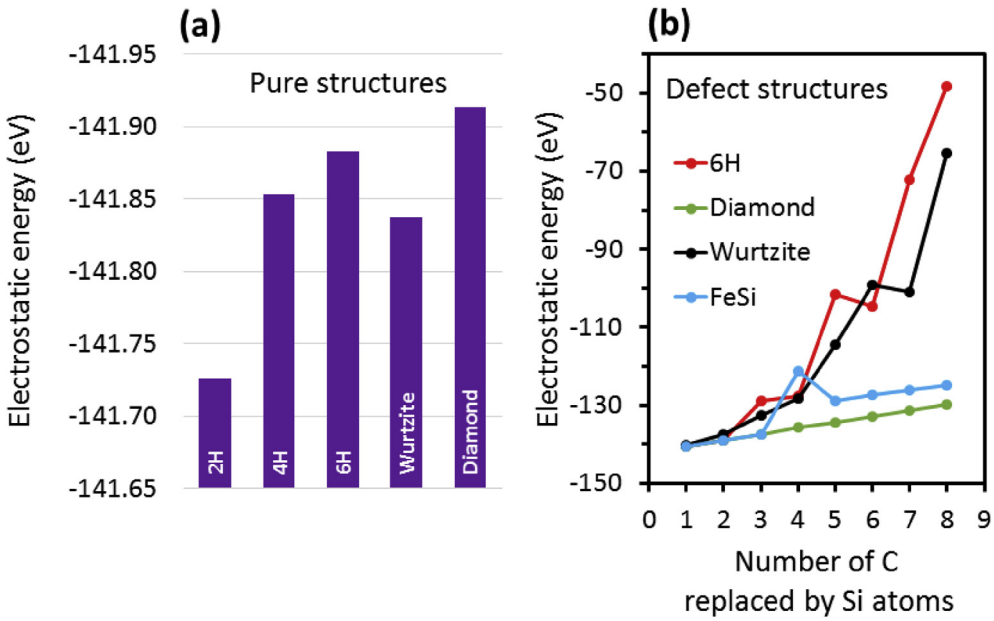

Fig. 4. The electrostatic energies for (a) pure and (b) defect structures of SiC.

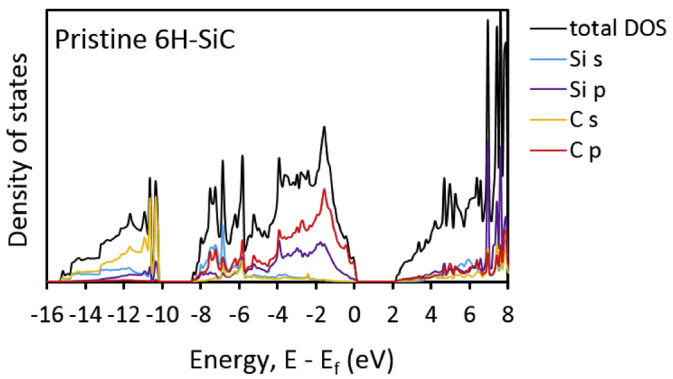

Fig. 5. GGA calculated density of states (DOS) for the 6H structure of SiC. The DOS is given in arbitrary unit. The Fermi level is set at 0 eV.

diamond, FeSi, Wurtzite and 6H SiC structures as C atoms are replaced by Si atoms. The reduction of electrostatic energy is the highest in the 6H structure which is about 65.63% for one to eight Si substitution whereas it is only 7.62% in the diamond structures. In fact, both the hexagonal structure, wurtzite and 6H showed similar electrostatic energy reduction

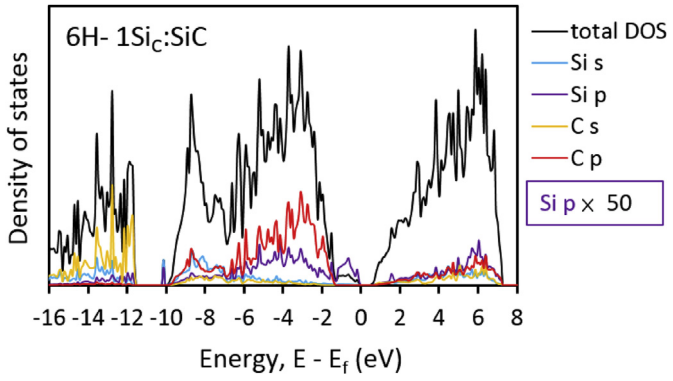

Fig. 6. GGA calculated density of states (DOS) for the 6H structure of 1Si$_C$:SiC. For better visualization, Si *p* is multiplied by 50; because of this magnification of high Si *p*, near Fermi level partial Si *p* DOS appears to be higher than total DOS. The DOS is in the arbitrary unit and the Fermi level is set at 0 eV.

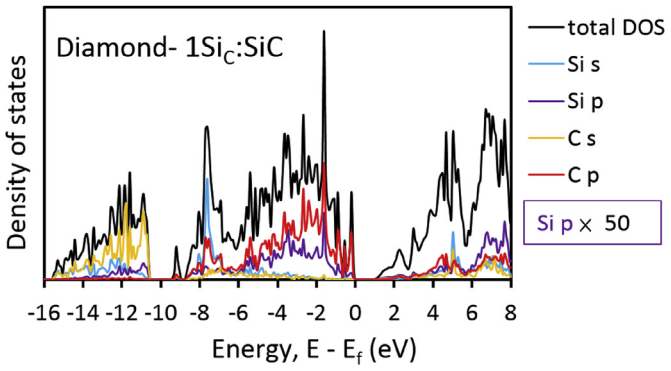

Fig. 7. GGA calculated density of states (DOS) for the diamond structure of 1Si$_C$:SiC. For better visualization, Si *p* is multiplied by 50. The Fermi level is set at 0 eV.

than the cubic structures, diamond and FeSi. This analysis suggests that the reason for the stability of 6H *n*Si$_C$:SiC structure is the stronger covalent bonding enhances in its environment rather than the ionic bonding.

3.4. The density of states (DOS)

For brevity, we have presented four density of states plots in this section to show how Si doping at C sites introduces new states near the Fermi level. Fig. 5 shows the total and partial density of states (DOS) plot for pristine 6H–SiC. The top of the valence band, valence band maximum (VBM), has the main contribution from C-*p* orbitals along some Si-*p*. As expected, the top part of the valence band, namely -4 eV–0 eV shows strong Si–C hybridization. At the VBM the *s/p* hybridization is suppressed

Table 9
The GGA band gap of diamond, FeSi, wurtzite, and 6H structures of pure and silicon-rich silicon carbides.

Structure	Diamond	FeSi	Wurtzite	6H
SiC	1.391	1.275	2.401	2.034
Si$_C$:SiC	0.773	0.773	0.590	0.418
2Si$_C$:SiC	0.240	0.675	0	0.239
3Si$_C$:SiC	0.162	0.064	0	0

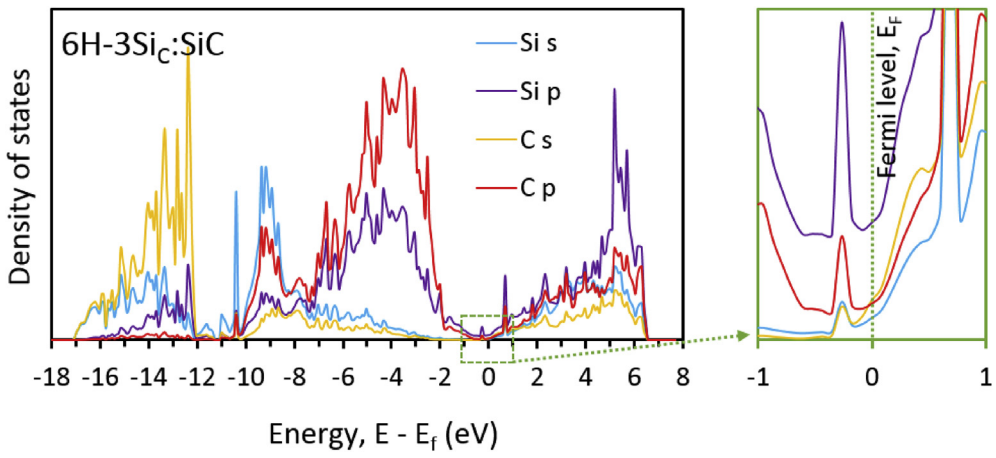

Fig. 8. GGA calculated density of states for 6H–3Si$_C$:SiC (n = 3). The figure shows non-zero states at the Fermi level where dominant contribution is from Si *p* states. The GGA calculated band gap in this case is zero.

due to the part ionic nature of the Si–C bonding. Fig. 6 shows the total and partial DOS plot for 6H– 1Si$_C$:SiC. The substitutional Si-*p* band is now seen on top of the valence band. However, this is not a very localized defect band; rather the width is about 1.43eV. Fig. 7 shows the total and partial DOS plot for diamond 1Si$_C$:SiC structure. Unlike 6H–1Si$_C$:SiC, no dominant Si-*p* level is seen on top of VBM, rather very localized C-*p* bands at VBM is found. The nature of CBM in all of these plots did not change much.

Now it is important to discuss the band gap trend. Table 9 shows the band gap of different *n*Si$_C$:SiC structures. For pristine SiC band gap of 6H and diamond structures are 2.034 eV and 1.391 eV, respectively. Reported experimental band gap for these two are 3.02 eV and 2.20 eV, respectively [65]. As is expected the calculated DFT band gaps are under-estimated compared to the experimental band gaps. With one Si substitution band gaps reduced significantly, 0.418 eV and 0.773 eV respectively. For 6H *n*Si$_C$:SiC, from $n = 3$ the band gap reduced to zero due to the extra Si *s/p* hybridized states in the band gap (Fig. 8). At this GGA level of calculations, these bands create metal-like materials. However, for diamond structure, even though it becomes thermodynamically unstable from $n = 4$ (Table 4), it does have zero band gap at $n = 3$, probably because of its higher ionic bonding nature compared to the hexagonal structures. Even within hexagonal structures, wurtzite has zero band gap with $n = 3$, as the ionic contribution is lower than the 6H structure than that of $n = 4$.

3.5. Optical absorption coefficients

In this section, we present the optical absorption properties of pure and silicon rich 6H-Si$_x$C$_{1-x}$. Our GGA-DFT calculated optical absorption coefficients are presented in Fig. 9 and are calculated using the formula as given in ref. [60]. Note that the energy gaps here were calculated from DFT, hence are under-estimated as mentioned earlier. The figure shows the first significant peak for pure 6H–SiC is at 3.89 eV. When Si atoms are doped for C sites (6H– Si$_{1.04}$C and Si$_{1.40}$C), the first major peak shifts at lower photon energy range for both cases. It shows that for higher Si concentration, the first major peak moves at 1.14 eV for Si$_{1.40}$C. For a pure system, there are only two major peaks up to 5 eV whereas for a Si-rich system there are multiple peaks for the same photon energy range and there is an overall red shift for Si-rich systems. This indicates that a Si-rich system extends the absorption spectra toward the lower photon

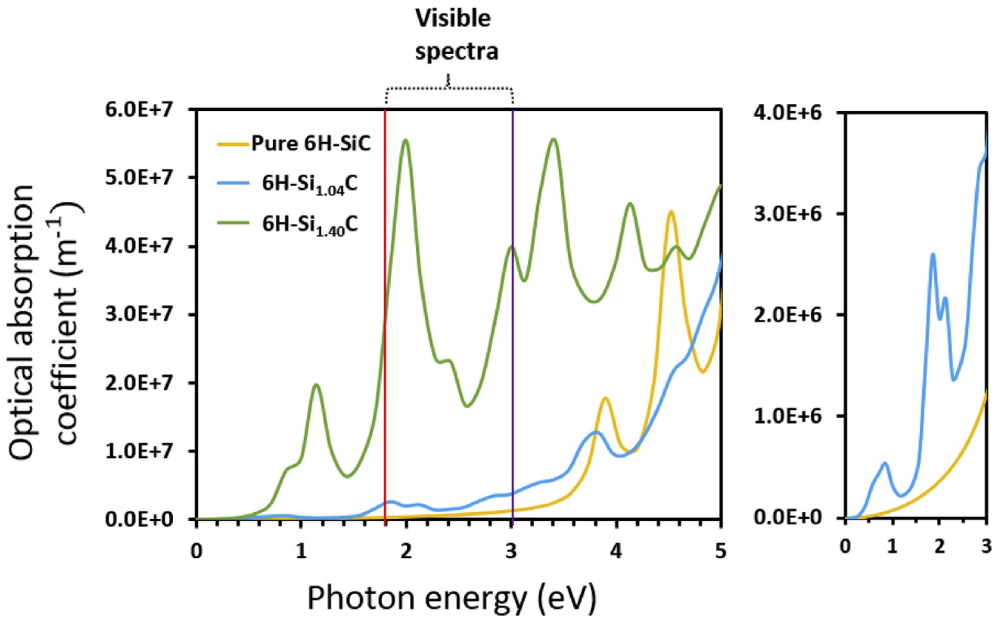

Fig. 9. GGA-DFT calculated optical absorption coefficients for pure and silicon rich 6H-Si$_x$C$_{1-x}$ systems. The right panel shows the magnified view of optical absorption from 0 – 3.0 eV.

energy region. Such red shift due to higher Si content was also found for silicon-rich Si_xC_{1-x} thin film photovoltaic solar cell [44]. Also, higher Si content enhances the overall photo absorption up to around 5 eV, and most particularly, the absorption increases significantly within the visible spectra as shown in Fig. 9.

4. Conclusions

We have examined the stability and the electronic properties of various polymorphs of silicon-rich silicon carbide phases with tunable bandgaps which could be suitable for photovoltaic applications. Different structures considered for this work were 2H, 4H, 6H, 8H, 10H, diamond, FeSi, and wurtzite structures of SiC. Within these structures, different numbers of carbon atoms were replaced by silicon systematically and studied within the density functional theory framework. We found that for pristine SiC, 6H and diamond structures have comparable stabilities. However Si-rich SiC favors hexagonal structures. The substituted Si atoms prefer to be near to each other rather than spread out randomly. Also, we have found that it is better to choose the extra silicon atoms to be on the same layers symmetrically distributed along the hexagonal lattice a and b directions to get energetically favorable structures. From electronic structure calculations, it was found that near the Fermi level the most contributions come from Si and C *p* orbitals. Also, we noticed that *s* and *p* orbitals in some structures have strong hybridization in the conduction bands. Within the scope of our study, 6H (or hexagonal) structures show more covalent nature than the diamond (or cubic structures). In addition, our optical absorption calculations show that Si-rich 6H–SiC shifts its absorption spectra toward lower photon energy region than its pure phase, and in the visible range the absorption coefficients are very high compared to the pristine SiC.

Declarations

Author contribution statement

Noura D. Alkhaldi, Sajib K. Barman: Performed the experiments; Analyzed and interpreted the data; Contributed reagents, materials, analysis tools or data; Wrote the paper.

Muhammad N. Huda: Conceived and designed the experiments; Analyzed and interpreted the data; Contributed reagents, materials, analysis tools or data; Wrote the paper.

Funding statement

Muhammad N. Huda was supported by the National Science Foundation (USA) Award No. 1609811.

Competing interest statement

The authors declare no conflict of interest.

Additional information

No additional information is available for this paper.

Acknowledgements

MNH would like to thank Alireza Yaghoubi on the early discussion on Si-rich SiC structures. NDA acknowledges the support of the Saudi Arabian Cultural Mission and University of Hafr Albatin. We gratefully acknowledge the generous computations time awarded by the Texas Advanced Computing Center (TACC) and High-Performance Computing (HPC) center of University of Texas at Arlington.

References

[1] M.I. Kabir, N. Amin, A. Zaharim, K. Sopian, Effect of energy bandgap of the amorphous silicon carbide (a-Sic: H) layers on a-si multijuntion solar cells from numerical analysis, in: 11th WSEAS Int. Conf. Math. Methods, Comput. Tech. Intell. Syst. MAMECTIS '09, 8th WSEAS Int. Conf. NOLASC '09, 5th WSEAS Int. Conf. Control '09, July 1, 2009 - July 3, 2009, 2009, pp. 334–337.
[2] M. Willander, M. Friesel, Q.U. Wahab, B. Straumal, Silicon carbide and diamond for high temperature device applications, J. Mater. Sci. Mater. Electron. 17 (2006) 1.
[3] R. Cheung, Silicon Carbide Microelectromechanical Systems for Harsh Environments, Imperial College Press, 2006.
[4] M. Rashid, B.R. Horrocks, N. Healy, J.P. Goss, A.B. Horsfall, Optical properties of mesoporous 4H-SiC prepared by anodic electrochemical etching, J. Appl. Phys. 120 (2016).
[5] M.B.J. Wijesundara, R. Azevedo, Silicon Carbide Microsystems for Harsh Environments, 2011, p. 22.
[6] G. Chikvaidze, N. Mironova-Ulmane, A. Plaude, O. Sergeev, Investigation of silicon carbide polytypes by Raman spectroscopy, Latv. J. Phys. Tech. Sci. 51 (2014) 51–57.
[7] Z. Li, R.C. Bradt, Thermal expansion of the hexagonal (4H) polytype of SiC, J. Appl. Phys. 60 (1986).
[8] H. Abderrazak, E.S.B. Hadj Hmi, Silicon carbide: synthesis and properties, Prop. Appl. Silicon Carbide (2011) 361–388.
[9] I.C. Massey, Synthesis and characterization of crystalline silicon carbide nanoribbons, Proc. Int. Conf. Pump Turbine Des. Dev. (1976) 1264–1271.
[10] L. Malakkal, B. Szpunar, R.K. Siripurapu, J.A. Szpunar, Thermal conductivity of bulk and nanowire of cubic-SiC from ab initio calculations, Comput. Mater. Sci. 128 (2017) 249–256.
[11] W. Wondrak, E. Niemann, R. Held, R. Constapel, G. Kroetz, SiC devices for power and high-temperature applications, in: Ind. Electron. 1998. Proceedings. ISIE '98. IEEE Int. Symp. 1, 1998, pp. 153–156.
[12] S.W. Lee, S.D. Park, S. Kang, I.C. Bang, J.H. Kim, International Journal of Heat and Mass Transfer Investigation of viscosity and thermal conductivity of SiC nanofluids for heat transfer applications, Int. J. Heat Mass Transf. 54 (2011) 433–438.
[13] R.A. Andrievski Synthesis, Structure and properties of nanosized silicon carbide, Rev. Adv. Mater. Sci. 22 (2009) 1–20.
[14] P. Sukkaew, E. Kalered, E. Janzén, O. Kordina, Ö. Danielsson, L. Ojamäe, Growth mechanism of SiC chemical vapor deposition: adsorption and surface reactions of active Si species, J. Phys. Chem. C 122 (2018) 648–661.
[15] P. Zhu, M. Yang, Q. Xu, Q. Sun, R. Tu, J. Li, S. Zhang, Q. Li, L. Zhang, T. Goto, J. Shi, H. Li, H. Ohmori, M. Kosinova, B. Basu, Epitaxial growth of 3C–SiC on Si(111) and (001) by laser CVD, J. Am. Ceram. Soc. 101 (2018) 3850–3856.
[16] D.H. Nam, B.G. Kim, J.Y. Yoon, M.H. Lee, W.S. Seo, S.M. Jeong, C.W. Yang, W.J. Lee, High-temperature chemical vapor deposition for sic single crystal bulk growth using tetramethylsilane as a precursor, Cryst. Growth Des. 14 (2014) 5569–5574.
[17] A. Ellison, J. Zhang, J. Peterson, A. Henry, Q. Wahab, J.P. Bergman, Y.N. Makarov, A. Vorob'ev, A. Vehanen, E. Janzén, High temperature CVD growth of SiC, Mater. Sci. Eng. B 61–62 (1999) 113–120.
[18] O. Kordina, C. Hallin, A. Ellison, A.S. Bakin, I.G. Ivanov, A. Henry, R. Yakimova, M. Touminen, A. Vehanen, E. Janzén, High temperature chemical vapor deposition of SiC, Appl. Phys. Lett. 69 (1996) 1456–1458.
[19] X. Li, G. Zhang, R. Tronstad, O. Ostrovski, Synthesis of SiC whiskers by VLS and VS process, Ceram. Int. 42 (2016) 5668–5676.
[20] X. Yao, S. Tan, Z. Huang, S. Dong, D. Jiang, Growth mechanism of β-SiC nanowires in SiC reticulated porous ceramics, Ceram. Int. 33 (2007) 901–904.
[21] M. Soueidan, G. Ferro, A vapor-liquid-solid mechanism for growing 3C-SiC single-domain layers on 6H-SiC(0001), Adv. Funct. Mater. 16 (2006) 975–979.
[22] Q. Lu, J. Hu, K. Tang, Y. Qian, G. Zhou, X. Liu, J. Zhu, Growth of SiC nanorods at low temperature, Appl. Phys. Lett. 75 (1999) 507–509.
[23] G. Urretavizcaya, J.M.P. Lopez, Growth of SiC whiskers by VLS process, J. Mater. Res. 9 (1994) 2981–2986.
[24] M. Sonoda, T. Nakano, K. Shioura, N. Shinagawa, N. Ohtani, Structural characterization of the growth front of physical vapor transport grown 4H-SiC crystals using X-ray topography, J. Cryst. Growth 499 (2018) 24–29.
[25] K. Eto, H. Suo, T. Kato, H. Okumura, Growth of P-type 4H–SiC single crystals by physical vapor transport using aluminum and nitrogen co-doping, J. Cryst. Growth 470 (2017) 154–158.
[26] P.J. Wellmann, T.L. Straubinger, P. Desperrier, R. Müller, U. Künecke, S.A. Sakwe, H. Schmitt, A. Winnacker, E. Blanquet, J.M. Dedulle, M. Pons, Modified physical vapor transport growth of SiC - control of gas phase composition for improved process conditions, Mater. Sci. Forum 483–485 (2005) 25–30.
[27] G. Dhanaraj, M. Dudley, R.H. Ma, H. Zhang, V. Prasad, Design and fabrication of physical vapor transport system for the growth of SiC crystals, Rev. Sci. Instrum. 75 (2004) 2843–2847.
[28] D. Hofmann, R. Eckstein, M. Kölbl, Y. Makarov, S.G. Müller, E. Schmitt, A. Winnacker, R. Rupp, R. Stein, J. Völkl, SiC-bulk growth by physical-vapor transport and its global modelling, J. Cryst. Growth 174 (1997) 669–674.
[29] J.W. Sun, V. Jokubavicius, L. Gao, I. Booker, M. Jansson, X.Y. Liu, J.P. Hofmann, E.J.M. Hensen, M.K. Linnarsson, P.J. Wellmann, I. Ramiro, A. Martí, R. Yakimova, M. Syväjärvi, Solar driven energy conversion applications based on 3C-SiC, Mater. Sci. Forum 858 (2016) 1028–1031.
[30] Y.C. Tsai, M.Y. Lee, Y. Li, M.M. Rahman, S. Samukawa, Simulation study of multilayer Si/SiC quantum dot superlattice for solar cell applications, IEEE Electron. Device Lett. 37 (2016) 758–761.

[31] I.A. Yunaz, K. Hashizume, S. Miyajima, A. Yamada, M. Konagai, Fabrication of amorphous silicon carbide films using VHF-PECVD for triple-junction thin-film solar cell applications, Sol. Energy Mater. Sol. Cells 93 (2009) 1056–1061.
[32] M. Konagai, Deposition of new microcrystalline materials, ??c-SiC, ??c-GeC by HWCVD and solar cell applications, Thin Solid Films 516 (2008) 490–495.
[33] S. Miyajima, K. Haga, A. Yamada, M. Konagai, Low-temperature deposition of highly conductive n-type hydrogenated nanocrystalline cubic SiC films for solar cell applications, Japanese, J. Appl. Physics, Part 2 Lett. 45 (2006).
[34] R.P. Raffaelle, N. York, S.G. Bailey, P. Neudeck, R. Okojie, N. Glenn, C.M. Schnabel, C. Western, Optical and Electrical of Sic Devices, 2000, pp. 1257–1260.
[35] Y. Tawada, H. Okamoto, Y. Hamakawa, A-SiC:H/a-Si:H heterojunction solar cell having more than 7.1% conversion efficiency, Appl. Phys. Lett. 39 (1981) 237–239.
[36] N. Alaal, V. Loganathan, N. Medhekar, A. Shukla, First principles many-body calculations of electronic structure and optical properties of SiC nanoribbons, J. Phys. D Appl. Phys. 49 (2016).
[37] H.C. Hsueh, G.Y. Guo, S.G. Louie, Excitonic effects in the optical properties of a SiC sheet and nanotubes, Phys. Rev. B Condens. Matter Mater. Phys. 84 (2011) 1–10.
[38] C. Persson, U. Lindefelt, B.E. Sernelius, Band gap narrowing in n-type and p-type 3C-, 2H-, 4H-, 6H-SiC, and Si, J. Appl. Phys. 86 (1999) 4419–4427.
[39] C. Persson, U. Lindefelt, Detailed band structure for 3C-, 2H-, 4H-, 6H-SiC, and Si around the fundamental band gap, Phys. Rev. B Condens. Matter Mater. Phys. 54 (1996) 10257–10260.
[40] H. Morkoç, S. Strite, G.B. Gao, M.E. Lin, B. Sverdlov, M. Burns, Large-band-gap SiC, III-V nitride, and II-VI ZnSe-based semiconductor device technologies, J. Appl. Phys. 76 (1994) 1363–1398.
[41] M.N. Huda, A.K. Ray, Carbon dimer in silicon cage: a class of highly stable silicon carbide clusters, Phys. Rev. A - At. Mol. Opt. Phys. 69 (2004), 011201R.
[42] M.N. Huda, A.K. Ray, Novel silicon-carbon fullerene-like cages: a class of sp3 - sp2 covalent-ionic hybridized nanosystems, Eur. Phys. J. D. 31 (2004) 63–68.
[43] M.N. Huda, A.K. Ray, Theoretical study of SiC nanostructures: current status and a new theoretical approach, J. Comput. Theor. Nanosci. 9 (2012) 1881–1905.
[44] C.-T. Lee, L.-H. Tsai, Y.-H. Lin, G.-R. Lin, A chemical vapor deposited silicon rich silicon carbide P-N junction based thin-film photovoltaic solar cell, ECS J. Solid State Sci. Technol. 1 (2012) Q144–Q148.
[45] L. Tsai, C. Lee, Y. Lin, G. Lin, A Si-rich SixCI-x based p-n junction photovoltaic solar cells optical gap (eV), IEEE (2011) 1232–1235.
[46] M.A. Ouadfel, A. Keffous, A. Brighet, N. Gabouze, T. Hadjersi, A. Cheriet, M. Kechouane, A. Boukezzata, Y. Boukennous, Y. Belkacem, H. Menari, Si-rich a-Si1-xCx thin films by d.c. magnetron co-sputtering of silicon and silicon carbide: structural and optical properties, Appl. Surf. Sci. 265 (2013) 94–100.
[47] C.H. Cheng, L.H. Tasi, G.R. Lin, All silicon carbide based p-i-n photovoltaic solar cells with conversion efficiency enhanced by detuning the composition ratio of i-SixC 1-x layer, Conf. Rec. IEEE Photovolt. Spec. Conf. (2013) 1343–1345.
[48] G.-R. Lin, T.-C. Lo, L.-H. Tsai, Y.-H. Pai, C.-H. Cheng, C.-I. Wu, P.-S. Wang, Finite silicon atom diffusion induced size limitation on self-assembled silicon quantum dots in silicon-rich silicon carbide, J. Electrochem. Soc. 159 (2012) K35.
[49] G. Kresse, J. Furthmüller, Efficient iterative schemes for ab initio total-energy calculations using a plane-wave basis set, Phys. Rev. B Condens. Matter Mater. Phys. 54 (1996) 11169–11186.
[50] G. Kresse, J. Furthmüller, Efficiency of ab-initio total energy calculations for metals and semiconductors using a plane-wave basis set, Comput. Mater. Sci. 6 (1996) 15–50.
[51] P.E. Blöchl, Projector augmented-wave method, Phys. Rev. B. 50 (1994) 17953–17979.
[52] P. Blöchl, From ultrasoft pseudopotentials to the projector augmented-wave method, Phys. Rev. B. 59 (1994) 11–19.
[53] J.P. Perdew, K. Burke, M. Ernzerhof, Generalized gradient approximation made simple, Phys. Rev. Lett. 77 (1996) 3865–3868.
[54] J. Paier, R. Hirschl, M. Marsman, G. Kresse, The Perdew-Burke-Ernzerhof exchange-correlation functional applied to the G2-1 test set using a plane-wave basis set, J. Chem. Phys. 122 (2005).
[55] K. Berland, V.R. Cooper, K. Lee, E. Schröder, T. Thonhauser, P. Hyldgaard, B.I. Lundqvist, van der Waals forces in density functional theory: a review of the vdW-DF method, Rep. Prog. Phys. 78 (2015) 1–41.
[56] F. RozpŁoch, J. Patyk, J. Stankowski, Graphenes bonding forces in graphite, Acta Phys. Pol. 112 (2007) 557–562.
[57] A. Jain, S.P. Ong, G. Hautier, W. Chen, W.D. Richards, S. Dacek, S. Cholia, D. Gunter, D. Skinner, G. Ceder, K.A. Persson, Commentary: the materials project: a materials genome approach to accelerating materials innovation, Apl. Mater. 1 (2013).
[58] R.T. Downs, M. Hall-Wallace, The American Mineralogist crystal structure database, Am. Mineral. 88 (2003) 247–250.
[59] K. Momma, F. Izumi, VESTA: a three-dimensional visualization system for electronic and structural analysis, J. Appl. Crystallogr. 41 (2008) 653–658.
[60] L. Dong, R. Jia, B. Xin, B. Peng, Y. Zhang, Effects of oxygen vacancies on the structural and optical properties of β-Ga_2O_3, Sci. Rep. 7 (2017) 40160.
[61] N. Shi, W. Bai, G. Li, M. Xiong, J. Yang, Z. Ma, H. Rong, FeSi Naquite, A new mineral species from Luobusha, Tibet, Western China, Acta Geol. Sin. 86 (2012) 533–538.
[62] G.L. Harris, Properties of Silicon Carbide, 1995.
[63] S. Komatsu, First-principles study of 8H- , 10H- , 12H- , and 18H-SiC polytypes, J. Phys. Soc. Japan 81 (2014), 024714.
[64] M.P. Marder, Condensed Matter Physics, second ed., 2010, pp. 295–319.
[65] J. Fan, P.K.-H. Chu, Silicon Carbide Nanostructures, Springer International Publising, 2014.